Optical Materials 94 (2019) 138–147

Contents lists available at ScienceDirect

Optical Materials

journal homepage: www.elsevier.com/locate/optmat

Controlling self-assembly of ultra-small silver nanoparticles: Surface enhancement of Raman and fluorescent spectra

Jamilur R. Ansari[a], Neelam Singh[a], Razi Ahmad[b], Dipankar Chattopadhyay[c], Anindya Datta[a,*]

[a] University School of Basic and Applied Sciences, Guru Gobind Singh Indraprastha University, Sector 16-C, Dwarka, New Delhi, 110078, India
[b] Center for Organic Electronics, Physics of Energy Harvesting Division, CSIR-National Physical Laboratory, Dr. K.S. Krishnan Road, New Delhi, 110012, India
[c] Department of Polymer Science and Technology, (CRNN), UCSTA, University of Calcutta, 92A.P.C. Road, Kolkata, 700009, West Bengal, India

ARTICLE INFO

Keywords:
Self-assembly
Diffusion-limited aggregation
pH-dependent fractal structure
Ag NPs
SERS
Enhanced photoluminescence

ABSTRACT

Resorcinol based reduction and capping of ultra-small colloidal silver nanoparticles (Ag NPs) optimally formed hydrogen bond driven clusters within the water-based solution. Large-area self-assembled fractal structures of Ag NPs aggregates were fabricated by solvent evaporation technique on silicon substrate. The final dried surface structures were found to be pH dependent which was adjusted to particular values after the optimal reduction of silver salt, capping of Ag NPs, followed by cluster formation at an optimum pH in the solution phase. These self-assembled surface structures show controlled enhancement of various surface optical phenomena such as Raman spectra of a model dye and luminescence of Ag NPs as a function of pH dependent fractal dimension of the resulting structures. The structure, morphology and various relevant optical properties of self-assembled fractals of Ag NPs were further established by combined use of X-Ray diffractometry (XRD), Scanning Electron Microscopy (SEM), Transmission Electron Microscopy (TEM), UV-Visible, photoluminescence and Raman spectroscopy analysis.

1. Introduction

Preparation of specific substrate which would be suitable for various surface enhanced phenomena such as surface-enhanced Raman spectroscopy, surface-enhanced photoluminescence spectroscopy is very challenging as these spectroscopies can be used for various processes in diverse fields of catalysis [1], bio-sensing and pH sensors [2,3], biology [4], food processing [5] and materials science [6]. To date various methods has been used to fabricate the SERS active substrates [7–9], such as top down lithographic techniques [10], chemical [11] and electro-chemical [12] deposition and thin film deposition by solvent evaporation [13] from colloidal suspension of metal nanoparticles [14] on cleaved mica wafer or silicon wafer [15]. The final properties of these SERS active substrates depend on the final size, shape, and inter-particle separation of the particles deposited on silicon substrate [16]. Attraction of silicon surface is immediate because of its possibility of integration with electronics. The easiest among all these processes is the deposition of colloidal suspension on silicon substrate. Not only the solution grown substrates are easy to prepare, but these bottom-up substrates can achieve very close inter-particle separation, critical for any surface enhancement, which is not easy to be achieved by top-down methods [17].

Drying of the colloidal solution on the substrate is a complex process, which results into various kinds of final arrangements of the colloidal materials on the substrate. In order to understand various factors influencing the formation of different kind of patterns on various substrates, a large number of simulations and experiments have been conducted [18]. Starting from a set of seminal works by Deegan et al. [19,20] large number of interesting works were done and the resulting structures were found to be dependent on the intrinsic characteristics of the nanoparticles, their species, shape, the polarity of the solvent involved, the surrounding properties such as electric, magnetic, or even macroscopic flow field [21]. The surface modifications along with the use of tactics of changing particle and base fluid can also lead to a variety of surface structures [22,23]. One such very interesting structure that results from drying of colloidal suspension on a substrate is fractal structure, which can form in various ways including self-assembly from a colloidal suspension. The localized dipolar excitations were observed directly on the rough nanostructured surfaces [20–26]. Fractals are structures which lack translational symmetry but show dilational symmetry. The roughness in ideal fractal can be scale invariant. But the real fractal-like structures, which might be dendritic,

* Corresponding author.
E-mail addresses: jransari.phd@gmail.com (J.R. Ansari), singh.neelam43@gmail.com (N. Singh), razi.nanotech@gmail.com (R. Ahmad), dipankar.chattopadhyay@gmail.com (D. Chattopadhyay), anindya_datta@yahoo.com (A. Datta).

https://doi.org/10.1016/j.optmat.2019.05.023
Received 26 April 2019; Received in revised form 13 May 2019; Accepted 13 May 2019
Available online 27 May 2019
0925-3467/

are usually self-similar within an effective length scale [19,20]. Such an arrangement has a consequence for our main motivation to have surface enhanced phenomena [27–29], which can lead to various kind of sensing devices. Electromagnetic waves cannot travel translationally on these kinds of structures. So, during normal mode excitations, while the fractal volume is not excited, superhot localized spots are created depending on the geometry and excitation wavelength and polarization of the light used. The hotspot created, however, cannot be described by conventional surface-plasmon wave's polaritons or by independent localized surface plasmon. Light with proper wavelength, when used, can enhance the average electromagnetic field intensity for individual noble metal particles. If the excitation wavelength is much bigger than the individual particle, then these resonances are entirely dipolar in nature. In fractal aggregates, these dipoles couple and convert these enhancements localized at hot spots to become enormous [30,31]. This extremely high surface enhancement [32] makes the fractal structures interesting. In our case, we have modified the process of formation of Ag NPs in suspension using resorcinol [27]. This method is known to produce high yield Ag nanoparticles. The modified method is aimed at creating a situation, where on drying, the fractal dimension of the dried structure can be controlled. Therefore, the impacts of the fractal dimension on various surface enhancements were studied in details. This simple method and its results along with detailed characterization studies are reported in this paper.

2. Experimental

2.1. Material and methods

Silver nitrate ($AgNO_3$), resorcinol ($C_6H_6O_2$), hydrogen chloride (HCl), nitric acid (HNO_3), ammonia (NH_3), hydrogen peroxide (H_2O_2) and ethanol (C_2H_5OH) were purchased from Merck and Rhodamine 6G (R6G), sodium hydroxide (NaOH) solution were procured from Alfa Aesar. The chemicals were of analytical grade and were used without purification. Ultra-pure water (18.2 MΩ cm resistance) from Milli-Q was used for the synthesis. The Teflon coated magnetic beads and the glassware were carefully cleaned in aqua regia solution (HNO_3: HCl: 1:3) and then properly washed with Milli-Q water under sonication and finally dried in vacuum oven. Ag NPs were formed as suspension within water and capped with resorcinol in order to achieve reduction of silver salt and control the size. Based on the pH of the solvent, they form a clustered structure [27]. By keeping the concentration of $AgNO_3$ constant at an optimum value, the concentration of resorcinol was varied in order to obtain various Ag NP sizes. The individual isolated Ag NPs were determined by UV–Vis spectroscopy. Clustering of Ag NP was obtained by varying the pH of the suspension. UV–Vis spectroscopy can provide the signature of the individual isolated Ag NPs and their cluster formation [33]. From the band gap determined from UV–Vis spectroscopy, one can find out the particle size of the Ag NPs. A few representative results are discussed in the UV–Vis spectroscopic analysis. The structural analysis of Ag NPs was performed by X-ray diffraction and transmission electron microscopy. When casted on silicon substrate, these suspensions form Ag fractals. In this work, we found out the optimized best possible results in terms of surface enhancements shown in the photoluminescence and Raman spectroscopy. The results are presented in the following sections with their possible explanation.

2.2. Characterization for self-assembled fractal structure of Ag NPs

UV–Vis absorbance spectroscopy (Shimadzu UV-2401 PV) was used to obtain the SPR of the samples. X-Ray diffraction (XRD) patterns of the self-assembled structure of Ag NPs samples were obtained using PANalytical X-Ray diffractometry (X'pert PRO). TEM-JEOL-JEM-2100 was used to analyze the microstructure and morphologies of the samples by Transmission Electron Microscopy (TEM). It was operated at an accelerating voltage of 200 kV and was equipped with Energy-dispersive X-ray spectroscopy (EDX) and Selected Area Electron Diffraction (SAED). Scanning Electron Microscopy (SEM) (EVO 18 SEM Carl Zeiss) was used to capture the images of these structures and their fractal dimensions were analyzed by Fraclac Version 2.5 (NILGS, NARO) and ImageJ software. Spectroflurolog (FL 3–11) was used to capture Photoluminescence (PL) spectra of the as-synthesized samples. Renishaw confocal laser Raman Spectrometry [INVIA (Gloucestershire, UK)] was used to study the Raman and SERS spectra resulting from the surface structures respectively.

2.3. Preparation of self-assembled fractal structure of Ag NPs

Self-assembled fractal structure of Ag NPs was synthesized by the route previously reported by T. Pal et al. [27] with slight modifications. In brief, an aqueous solution of Ag NPs was prepared using 10 mL of aqueous resorcinol (100 mM) solution. 0.5 mL of aqueous $AgNO_3$ (5 mM) solution was then dropped into the solution and was allowed to mix under constant stirring. Lastly, 10 mL of aqueous NaOH (0.5 mM) was added drop-wise for 20 min and was allowed to stir further at room temperature. Upon adding $AgNO_3$ solution it instantly changed to yellow color, indicating the formation of Ag NPs. After stirring for 30 min the solution turned reddish-yellow indicating the aggregates formation of Ag nanoparticles. Further, there was no change observed which leads to the completion of the reaction. The pH of the entire reaction was kept at 8, as this was reported to be the optimum pH for cluster formation in the solution and fractal formation on the substrate while drying [27]. Thereafter, we changed the pH of the solution both to more basic and acidic direction. The idea was to allow an initial reduction of silver salt followed by capping due to the presence of resorcinol. We changed the pH after this process was complete so that this process of metal nanoparticles formation and their adequate capping is not affected. However, changing the pH after this process is expected to affect the already formed cluster in the solution as well as the drying process. The changes became obvious in UV–Vis spectroscopic study of the pH-dependent solution and the corresponding solutions those were cast and dried on substrates [34]. The details of the results and their possible reasons are discussed at proper sections.

As synthesized samples were washed thrice using ultrapure water (Milli-Q), and finally sonicated to be used for various characterizations. As synthesized samples at (i) pH 8 in solution phase, and (ii) re-dispersed samples of 10 wt% in water are depicted in Fig. 1. Along with this, emission under (iii) daylight exposure and under UV lamp at (iv) 254 nm and (v) 365 nm, are shown in Fig. 1 and Ag NPs casted on glass slide and their emission in UV lamp before and after drying in daylight, at 254 nm and 365 nm is shown Fig. A1. When the sample solutions were allowed to complete full reaction, various stages of nano-silver formation can be observed. Initially, Ag NPs were known to form in a non-clustered capped form [27]. If the reaction was allowed to go forward, after the completion of the reaction, the pH of the solution comes down to ~6. It was then adjusted to 8 at room temperature. At this pH, silver cluster forms due to the hydrogen bonding between various capped Ag nanoparticles [35]. As hydrogen bonding is not so strong, this cluster formation is reversibly tunable based on the pH of the suspension [27]. After the cluster formation was complete, which was determined by UV–Vis spectroscopy, we adjusted the pH from 3 to 11. The probing of the pH modified suspension by UV–Vis spectroscopy showed changes in the plasmonic peaks belonging to the silver clusters, which implies pH based reversible changes in cluster size and in the inter-particle separation of Ag nanoparticles. In order to study the different size of Ag NPs, we have varied the concentration of resorcinol, keeping the concentration of silver salt constant and it has been optimized at pH = 8. By varying the concentration of resorcinol from 100 mM to 25 mM, the particle size has been varied.

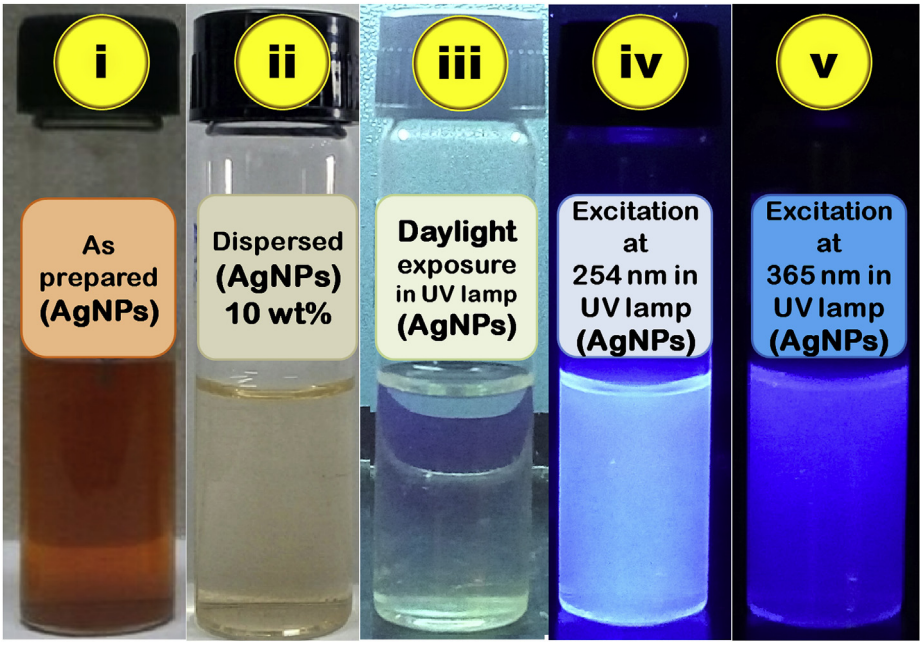

Fig. 1. (i) As synthesized samples at pH 8 in solution phase, and (ii) re-dispersed samples of 10 wt% in water. Along with this, emission under (iii) daylight exposure and under UV lamp at (iv) 254 nm and (v) 365 nm.

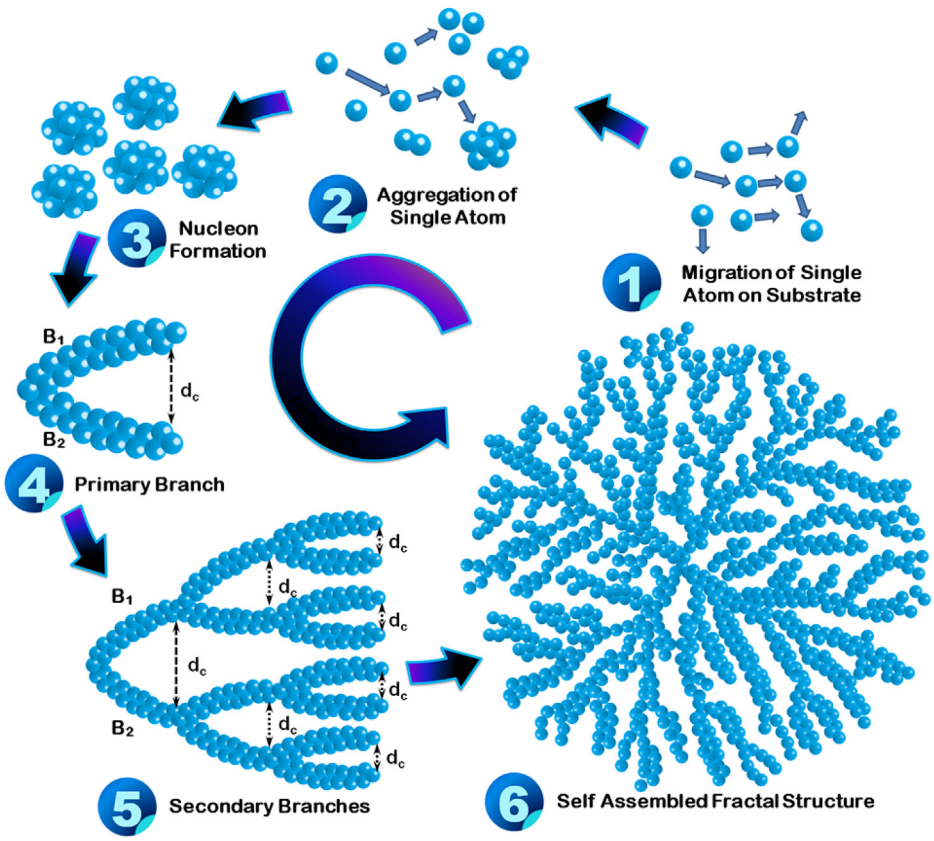

Scheme 1. Schematic illustration of the DLA mechanism: Initially single atoms migrated on the substrate which aggregate to form nucleon of Ag NPs around pinning centers. Then primary branches (B_1 and B_2) grow from the nucleon and shortly secondary branches grow automatically from the primary branch. With increasing separation (d) between the adjacent branches, the potency of the energy barrier is reduced. As a result, a critical distance (d_c) exists, beyond which Ag nanoparticles break the energy barrier to reach the surface. Thus, the self-assembly pattern mechanically assembled themselves as a fern-like fractal structure. This scheme works the best when pH of the solution was 8, which promotes DLA based growth. When pH is away from 8, many pinning centers form on a silicon wafer. As a result, the growth of structures on the wafer shifts away from the DLA limit.

2.4. Preparation of super-hydrophilic surfaces at silicon wafers

Silicon wafers were cut into 2 × 2 mm in size and were cleaned to achieve super hydrophilic surfaces as suggested by Kern and Puotinen [36,37]. The processed silicon wafer is super hydrophilic having contact angles < 5° (although the measured value is considered as zero) [38]. Then the silicon wafers were sonicated for 20 min with a mixture of ethanol and DI water in the same ratio and finally sonicated for 20 min with ethanol to remove unbound monomers from the surface. For SEM analysis, Ag NPs was cast drop-wise and allowed to dry in a vacuum and the drying process is as shown in Fig. A2.

When these suspensions were cast and dried on a silicon wafer,

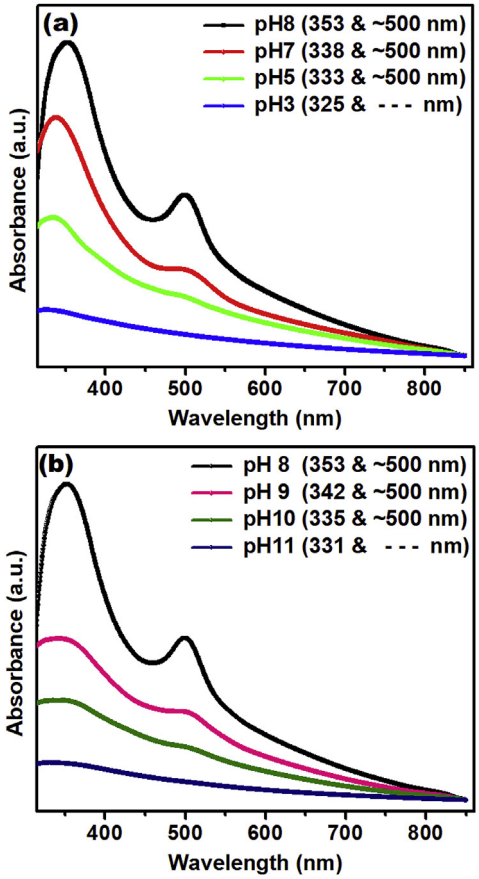

Fig. 2. UV–Visible absorption spectra of the as-synthesized self-assembled fractal structure of luminescent Ag NPs on glass slides with varying pH from (a) pH = 8 to 3 and (b) pH = 8 to 11.

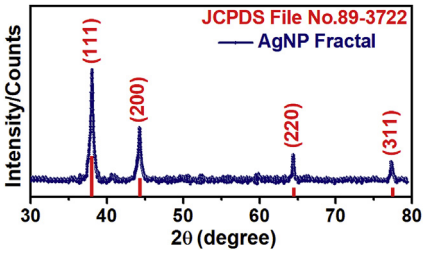

Fig. 3. XRD pattern of self-assembled fractal structure of Ag NPs.

which was usually covered with a native thin SiO_2 layer, the reacting species in the solution due to addition of acid/base were likely to react with the native oxide and create pinning sites. Our motivation to do so was to influence the drying process to move away from the so-called "DLA" mediated structure that finally forms on the silicon surface. The formation of the final structure is a very complex process. The collapse of the three dimensional structures those formed in the liquid to two dimension [39,40] when cast and restructuring while getting dried, were further influenced by the pH of the suspensions due to creation of pinning centers on silicon, change in cluster structure in the liquid by the effect of pH on hydrogen bonding [35,41,42] and influence on the electrostatic force by pH [27].

2.5. Surface enhanced Raman Spectroscopy (SERS) measurements

Raman scattering measurements were done under an ambient condition with confocal laser Raman spectrometry with an excitation source of 785 nm. The samples were immersed in the Rhodamine 6G (R6G) solution for 30 min, followed by rinsing with ethanol and drying under vacuum before SERS spectra were recorded.

3. Results and discussions

In the typical synthesis of silver nanoparticles, Ag ions are reduced by resorcinol in the presence of sodium hydroxide. When the size of nanoparticles approaches the Fermi wavelength of an electron (i.e. 0.5 nm for noble metals), luminescent Ag nano-clusters is formed [43]. Self-assembled fractal structure of Ag nanoparticles was characterized using XRD, SEM, TEM/HRTEM, UV–Visible absorption, PL and Raman spectroscopy. SERS was studied by Raman Spectroscopy. Fraclac and ImageJ software were used to establish the fractal dimension (F_D) of the resulting structures on silicon surfaces.

The morphology of the fractal structures was studied by SEM and TEM/HRTEM. By the addition of resorcinol, the nanoparticles were assembled in a close-packed assembly by the formation of hydrogen bonding at a particular concentration, 0.5 mM of NaOH [44].

Due to the impact of resorcinol, an electric charge (highly negative) exists on the surfaces which also abstain from oxidation and very small sizes of Ag NPs (particularly in the range of 1–3 nm) are formed. The overall reaction mechanism is given as.

$$2C_6H_6O_2 + 2Ag^+ = 2Ag^0 + (C_6H_6O_2 - C_6H_6O_2)$$

The schematic illustration of the self-assembled fractal structure of luminescent Ag NPs is as shown in Scheme 1.

3.1. UV–Vis analysis of self-assembled fractal structure of Ag NPs

In order to study the different size of Ag NPs, we have varied the concentration of resorcinol, keeping the concentration of silver salt constant and it has been optimized at pH = 8. By varying the concentration of resorcinol from 25 mM to 100 mM, the particle size has been varied. At higher concentration (1.0 M) of resorcinol, Ag NPs were precipitated [27]. The initial testing was done by UV–Vis absorption spectroscopy. The typical absorption spectrum for three different concentration of resorcinol is shown in Fig A3(c), when the particles form as isolated individual nanoparticles. The cluster formations followed by fractal formation on silicon substrate are found to be function of resorcinol concentration. At lower concentrations, Ag NPs do not form clusters. No fractal formations were observed for these structures. A single hump was observed with the plasmonic peak red shifting to 432 nm and 438 nm corresponding to particles size 12 nm and 20 nm respectively [27]. We see that, Ag NPs forms dual peak at λ_{max} = 342 nm and 490 nm at 100 mM concentrations of resorcinol as shown in Fig A3 (a-b). Further, the formation of self-assembled fractal structures was also confirmed by SEM images, as shown in Fig. 4.

By appropriate choice of metals, dielectric and geometries of the colloid, the spectral position can be tuned in the SPR range [45]. The absorbance spectra of the self-assembled fractal structure of luminescent Ag NPs were studied using UV–Vis absorbance spectroscopy and two maxima peaks were observed at 353 nm and ~500 nm as shown in Fig. 2. With varying pH from 8 to 3 and 8 to 11, we see that the λ_{1max} blue shifts while λ_{2max} broadened at ~500 nm and finally diminishes at pH = 3 and 11 respectively as shown in Fig. 2(a) and (b). It is also supported by the corresponding variation of the fractal dimension and SEM morphologies of the samples at respective pHs. The noble metal in the form of isolated nanoparticles shows plasmonic resonance based band and for Ag NPs it appears near ~410 nm in a water medium. The exact position and shape of this peak depend on the shape and size of the nanoparticles and the dielectric permittivity of the surrounding medium. However, in general, with the growth in size, the plasmonic peak shows redshift. When there is clustering of such nanoparticles in the solution, the plasmonic response of one particle gets coupled to other plasmons in different particles and a coupled plasmonic oscillation of the aggregates originates, depending on the mutual orientation

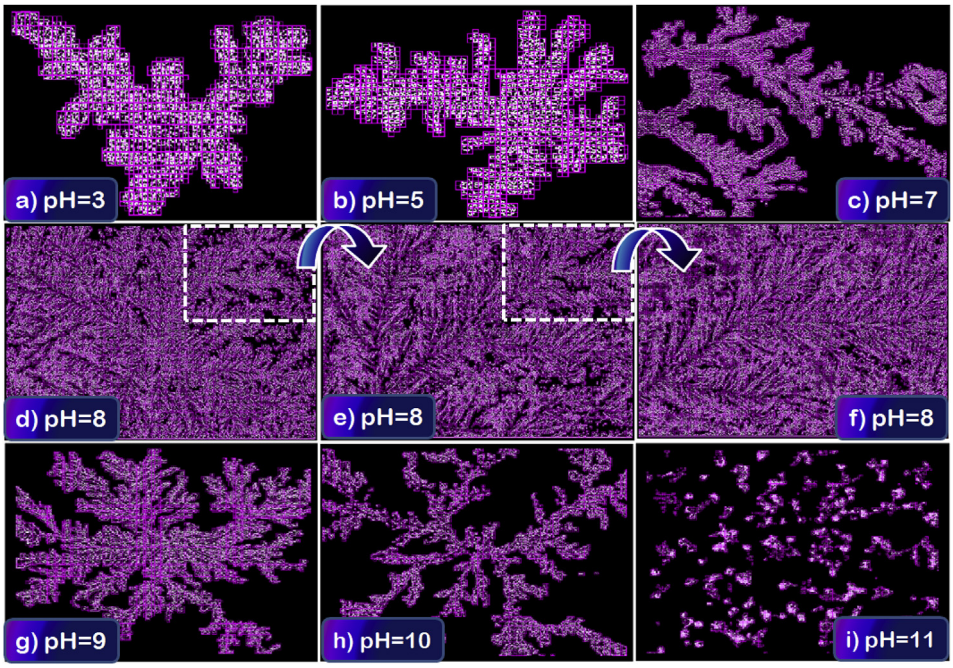

Fig. 4. SEM images of self-assembled fractal structure of Ag NPs at pH = 3 to 11 is divided into a number of boxes that covers the smallest possible fractal element. The graph depicts the overall boxes count required to wrap the fractal pattern as a function of 1/e.

of the individual particles within the aggregate [40]. With red-shift of dipole resonance, there is the growth of quadrupole resonance, which also shows red-shift with an increase of the size of individual nanoparticle. However, the contribution of quadrupole resonance is small, and the nature of the plasmonic resonance is therefore essentially dipolar [27,39]. So, in addition to plasmonic peak due to individual particles, a second peak near 500 nm grows which is of dipolar in nature for optimized concentration of resorcinol [27].

3.2. XRD analysis of self-assembled fractal structure of Ag NPs

The crystallographic structure of as-synthesized self-assembled fractal structure of Ag NPs was recorded using powder XRD as shown in Fig. 3. The observed peaks (111), (200), (220) and (311) are indexed to the plane of face-centered cubic structure (JCPDS File No. 89–3722) and are consistent with their corresponding bulk counterpart [46], confirming the formation of Ag NPs. The average crystallite size calculated by Scherer's formula was found to be 1.82 nm. We know that Ag colloid is extremely unstable especially due to the surface oxidation and random aggregation of Ag NPs. In our case, Ag nanoparticles surface is capped by resorcinol monolayer, which prevents the aggregation, based increase in the size of the nanoparticles or surface oxidation of Ag NPs. TEM/HRTEM image also confirms the characteristic diffraction peaks of Ag nanoparticles.

3.3. Scanning electron microscopy (SEM) and fraclac analysis of self-assembled fractal structure of Ag NPs

SEM was incorporated to analyze the surface morphology of the nanoparticles as shown in Fig. 4, which confirms the formation of the self-assembled fractal structure of luminescent Ag nanoparticles on the silicon wafers. The fractal pattern can be analyzed as an index of fractal dimension (F_D) by describing their convolution in the ratio of change in detail to that of scale. For the self-assembled system, F_D provides an idea about the structural complexity and its efficiency, specifically in terms of covered surface area. F_D is calculated by the box and counting method as it has proved to be of sufficient accuracy and efficiency as suggested by Barabasi [47]. Fig. 4 shows the SEM images of the self-assembled fractal structure of luminescent Ag NPs at pH = 3 to 11. The image of the fractal structure is divided into a number of boxes (N_d) of a fixed size (d) in such a way that it covers almost all the fractal structure to any scale to get the overall dimension by analyzing each and every box iteratively. The graph depicts the overall boxes count required to wrap the fractal pattern as a function of $1/\varepsilon$ (which is the inverse size of the box).

Fractal dimension was calculated by Fraclac Version 2.5 software developed by NILGS, NARO and ImageJ [48,49]. A linear fit has been plotted for the logarithmic plot (N_d) vs inverse of the box size ($1/\varepsilon$) to determine the value of fractal dimension (F_D) from the fractal structure. A prototype of each sample of pH = 3–11 has been chosen which represents the entire structure so as to analyze the fractal properties. All the data points of the fractal structures correspond to the linear fit and are almost in a straight line. The fractal dimension (F_D) was calculated from the slope of the linear fit. Fig. 5 depicts SEM images of the self-assembled fractal structure of Ag nanoparticles at pH varying from 3 to 11. It was found that when pH = 3, 5, 7, 8, 9, 10 and 11 the F_D was 1.62, 1.68, 1.71, 1.89, 1.76, 1.65 and 1.56 respectively. These images reveal the evolution of the self-assembled fractal structure of Ag NPs when pH was 8 and while increasing and decreasing pH beyond 8 the fractal starts splitting into smaller fractals and subsequently the fractal dimension decreases. We have varied the pH by varying the concentration of HNO_3 and NaOH for acidic and basic medium.

When HNO_3 and NaOH are in excess in the solution, their reaction with the native oxide on silicon surface creates more pinning centers. The surface itself also changes its nature. In acidic condition, the surface becomes more hydrophobic while for the basic condition, it behaves hydrophilically. Although we started with a hydrophilic surface, the addition of these conditions changes the nature of the surface based on pH dynamically. So all these conditions really affect the way the random walkers can redistribute themselves on the surface.

From the SEM morphology, it appears that with increasing pH from 3 to 8 and decreasing pH from 11 to 8, the branching of fractal structures increases. The change in the fractal dimension can be attributed to a change in pH of the solution. Also, with variations in pH from 3 to 8 and 11 to 8, the zeta potential is known to increase and the protonation tendency to decrease, leading to change in fractal structured patterns

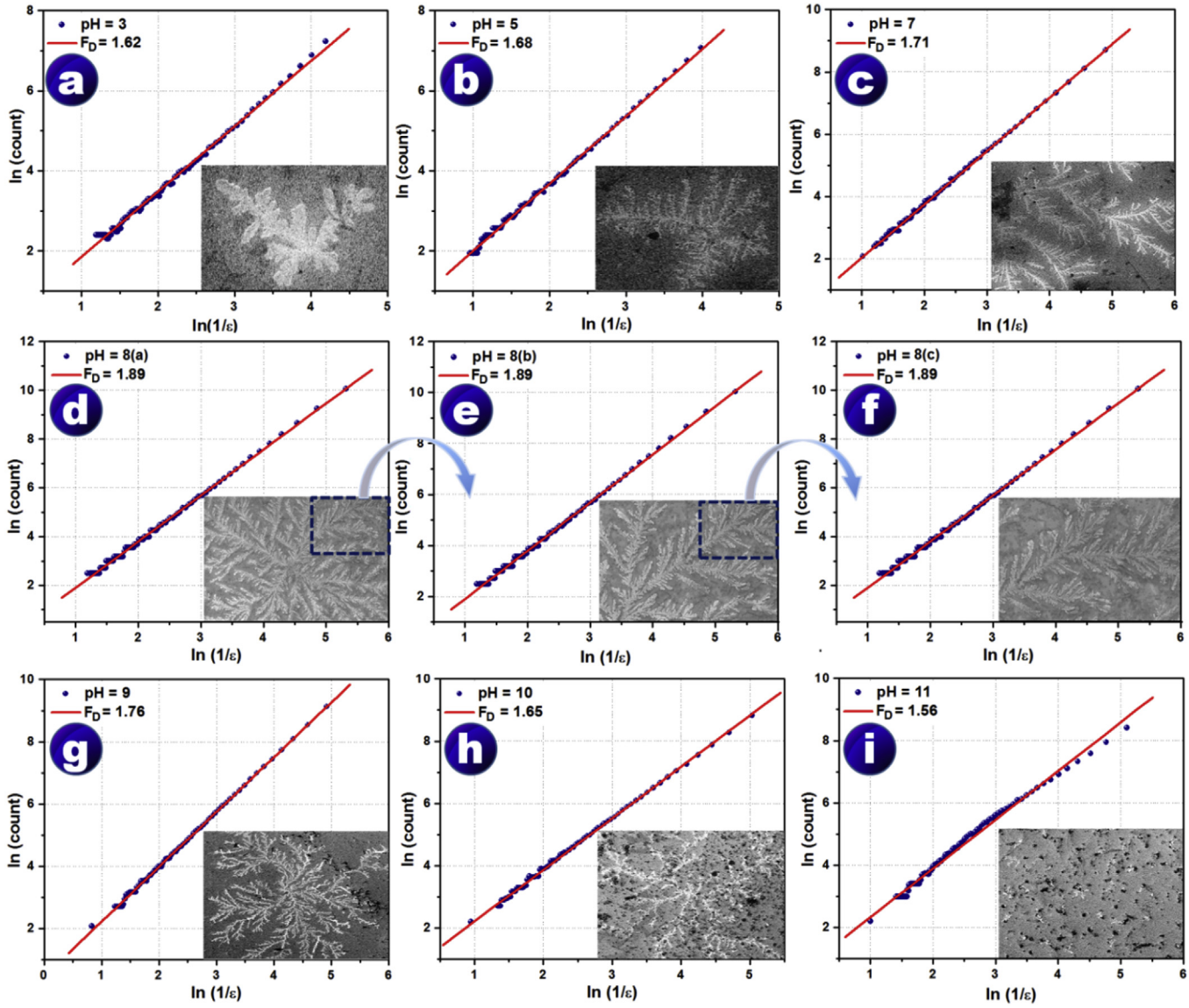

Fig. 5. SEM images at pH varying from 3 to 11 and their corresponding slopes depict the fractal dimensions FD.

[50].

3.4. Transmission electron microscopy (TEM) analysis of self-assembled fractal structure of Ag NPs

Fig. 6 depicts the TEM/HRTEM microstructures and morphologies of the as-synthesized Ag nanoparticles which confirm the formation of the self-assembled fractal structure of luminescent Ag nanoparticles. Fig. 6(a) show TEM images of the self-assembled fractal structure of Ag NPs on the carbon coated grid. Some individual Ag NPs as well as agglomerated nanoparticles of approximately 2.5 nm in size, which forms the self-assembled fractal structure of approximately 1000 nm in length. The formation of a fractal structure on the TEM grid depends on the concentration of the sample cast on the grid surface. It appears that self-assembled fractal structure formed when the sample was dried on the TEM grid and such formation of the fractal structure has previously reported by Magdassi and are well dispersed. Fig. 6(b) shows the microstructure of Ag NPs which are nearly spherical and are well dispersed. A histogram was plotted for the observed 320 nanoparticles and the average diameter was found to be 2.5 nm, as plotted in Fig. 6(c). Fig. 6(d) shows a high-resolution TEM image of the fractal structure, where lattice fringes are visible. Fig. 6(e) shows a further magnified highly crystalline image of the as-synthesized Ag NPs. We have further calculated the lattice fringes to be 0.24 nm [51] corresponding to (111) inter-planar spacing of Ag NPs with face-centered cubic structure. SAED pattern from the self-assembled fractal structure of Ag NPs is shown in Fig. 6(f), which corresponds with the characteristic diffraction peaks of XRD. In Fig. 6(g), EDX spectra show only Ag signals, Cu being consciously eliminated, matched well with the XRD results.

3.5. Photoluminescence (PL) analysis of self-assembled fractal structure of Ag NPs

Radiative damping resulting from the spontaneous emission of the induced dipole (with initial rapid growth of emission which finally reduces the size of the induced dipole, thereby increasing the line-width of the plasmonic peak) competes with the depolarization of the radiation across the surface of the particle due to finite ration of its size to wavelength of the light used [39,40]. The depolarization changes due to an increase in particle size introducing red-shift.

A fractal object with dilational symmetry having normal mode oscillations, where the excitation is not uniformly distributed over the whole structure but concentrated at localized super-hotspots due to very narrow inter-particle separation within cluster-cluster aggregation

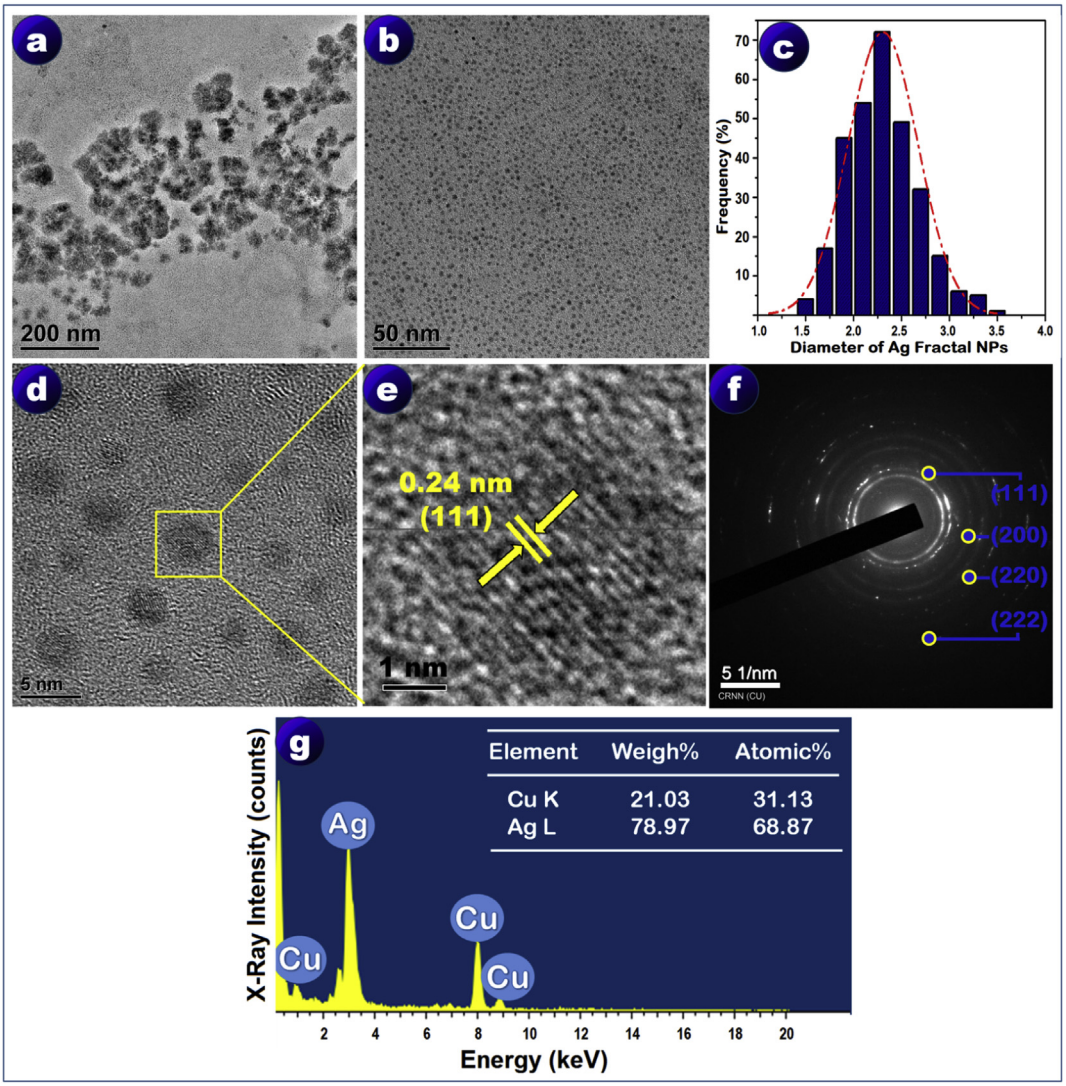

Fig. 6. (a) TEM micrograph (b) magnified TEM micrograph (c) size distribution histogram (d) high resolution TEM micrograph (e) lattice fringes of 0.24 nm corresponding to (111) planes (f) SAED pattern and (g) EDX of self-assembled fractal structure of Ag NPs.

involving collective motions of the conduction electrons. The clustering in these resorcinol based capped ultra-small nanoparticles developing into a final fractal-like structureis essentially controlled by the hydrogen bonding. The hydrogen bond forms in resorcinol when H^+ ion bonds with a negative ion or properly charged molecular group. pH change may cause changes in the charge of the group, but not necessarily breaks H-bonds [35]. If somehow the deprotonation changes due to change in pH, that will lead to change in the capability of forming a hydrogen bond. Even though the H-bonds are not completely broken there may be a rearrangement of the final structure.

Fig. 7(a) exemplifies the PL spectra of the self-assembled fractal structure of luminescent Ag nanoparticles, excited with a constant laser operational at 320 and 410 nm. The PL emission of luminescent silver nanoclusters was studied in detail to elucidate the origin of luminescence. The most important factor of the colloidal Ag NPs was that it exhibits excitation wavelength dependent photoluminescence [52]. As synthesized samples were cast on the glass slides and excited at 320 and 410 nm, the PL emission spectra were shown in Fig. 7(a). The PL spectra depict two sharp peaks at 411 nm and 544 nm at excitation energy 320 and 410 nm respectively, which were red-shifted with respect to SPR recorded using UV–Vis spectroscopy (see Fig. 6), indicating that the observed PL was obtained from electron excitations between discrete energy levels [43]. It was observed that two strong PL emission peaks were recorded when the luminescent Ag NPs were coated and dried on glass plates. The excitation wavelength dependent PL emission from the self-assembled fractal structure of Ag NPs implies that strong coupling exists between SPR and Ag nanoparticles [53].

The luminescent silver is usually very small and the luminescence generated by such nanoparticles is excitation wavelength dependent [53,54]. The luminescence is due to recombination of electron-hole pairs, electron being from sp conduction band from above Fermi level and holes being from the Fermi level belonging to d-band of these Ag NPs [52,55]. Even for some bigger Ag NPs, luminescence can be generated because of some different mechanism [56,57]. The transmission electron micrograph in Fig. 5 depicts a fractal structure that can be seen to be an assembly of very small Ag nanoparticles. Additionally, the fractal structure due to its dilational symmetry has superhot spots which provide electromagnetic enhanced fields [58]. Usually, these spots are located at the inter-particle separating space, which is very small and dependent on the hydrogen bonding which is active in this case. This weak bonding is tunable to the pH of the solution and is reversible in nature, which is reflected in the fractal dimension of the resultant structure. The special way in which our samples have been synthesized allows the capping to be complete. So, even in the clusters, although the Ag NPs are very close, physical touching of the silver surfaces belonging to various different Ag nanoparticles is not possible

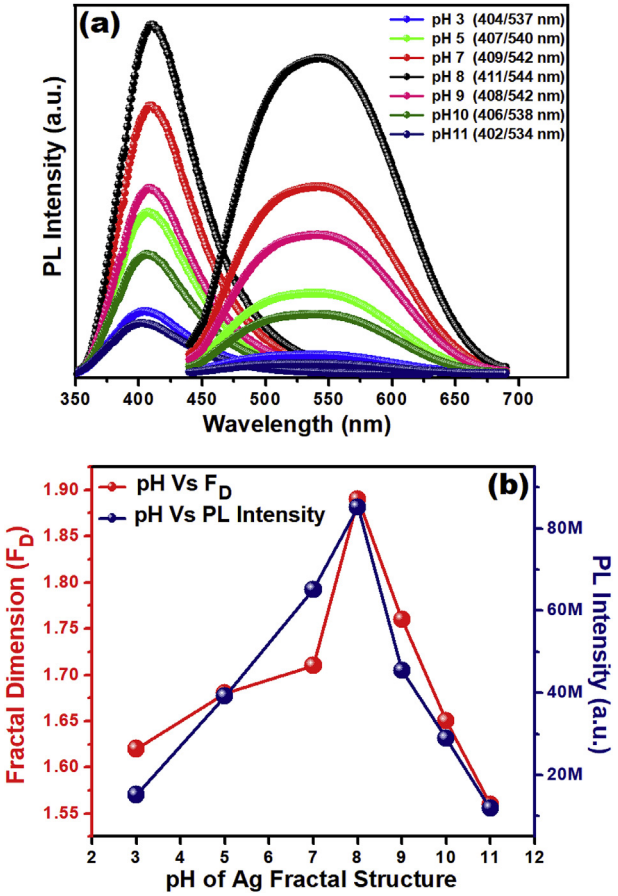

Fig. 7. (a) Photoluminescence emission spectra of self-assembled fractal structure of luminescent Ag NPs on glass slide at excitation energy of 320 nm and 410 nm. (b) Variation of fractal dimension (FD) and PL Intensity with varying pH from 3 to 11 of self-assembled fractal structure of luminescent Ag NPs.

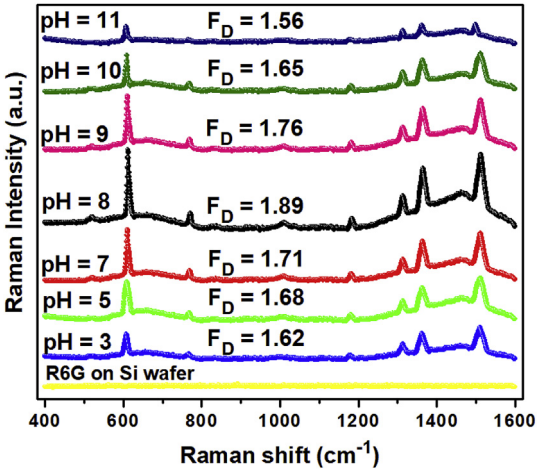

Fig. 8. Surface enhanced Raman spectra of the self-assembled fractal structure of luminescent Ag NPs with Rhodamine 6G (10-4 M) on a Si wafer and pH varying from 3 to 11 in the region 400-1600 cm-1.

as the capping layers always act as a barrier. The luminescence of Ag nanoparticles in this case, therefore, gets enhanced by the super-hot-spots of the fractal structure and is directly connected with the fractal dimension. A plot of fractal dimension (F_D)/PL intensity vs pH of Ag NPs was also obtained for the self-assembled fractal structure of luminescent Ag nanoparticles by varying the pH from 3 to 11. It was

Table 1
Raman shifts of the three SERS bands in the spectra of self assembled fractal structure of luminescent Ag NPs with pH and F_D varying from 3 to 11 and 1.89 to 1.56.s

pH of self-assembled fractalstructure of luminescent Ag NPs	Fractal dimension (F_D) of self-assembled fractal structure of Ag NPs	Observed SERS bands of self-assembled fractal structure of luminescent Ag NPs		
		~612 cm^{-1} band	~1365 cm^{-1} band	~1512 cm^{-1} band
		Peak Position	Peak Position	Peak Position
3	1.62	608.2	1362.7	1510.5
5	1.68	609.4	1363.2	1511.1
7	1.71	610.7	1363.9	1511.1
Optimum pH 8	**1.89**	**612.5**	**1365.1**	**1512.3**
9	1.76	610.7	1364.4	1511.7
10	1.65	609.4	1363.9	1511.1
11	1.56	607.6	1362.1	1506.9

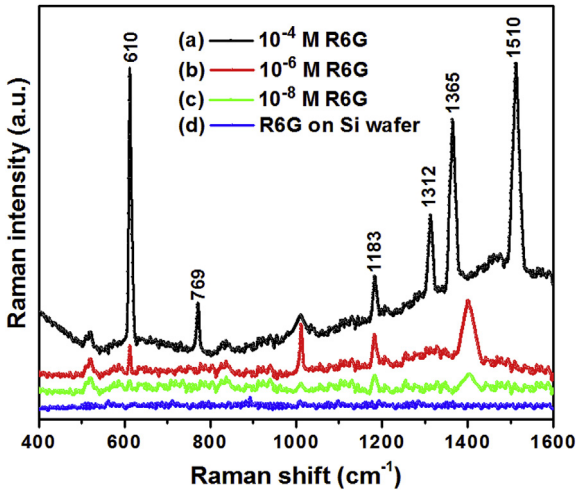

Fig. 9. SERS spectra of R6G with various concentrations: (a) 10-4 M, (b) 10-6 M, (c) 10-8 M on self-assembled fractal structure of luminescent Ag NPs and (d) 10-4 M on a silicon wafer. (For interpretation of the references to color in this figure legend, the reader is referred to the Web version of this article.)

observed that the fractal dimension decreases from 1.89 to 1.56 and correspondingly PL intensity also decreases with varying pHs as shown in Fig. 7(b).

3.6. SERS analysis of self-assembled fractal structure of Ag NPs

Fig. 8 shows surface-enhanced Raman spectra (SERS) of the self-assembled fractal structure of Ag nanoparticles on a silicon wafer with seven different pH varying from 3 to 11 in the region 400-1600 cm^{-1} with R6G (10^{-4} M).

At pH = 8 corresponding to $F_D = 1.89$ the peak position is highly intense and increasing or decreasing pH beyond 8 leads to decreasing intensity till $F_D \sim 1.6$ and the Raman bands blue shift at three positions from 612 cm^{-1} to 607 cm^{-1}, 1365 cm^{-1} to 1362 cm^{-1} and 1512 cm^{-1} to 1509 cm^{-1}. The variations in peak positions corresponding to pH and fractal dimension of the three prominent SERS bands are shown in Table 1.

We have used R6G samples of low concentrations (10^{-4} to 10^{-8} M) to verify the surface enhancement effect. Fig. 9 shows various peaks for R6G at around 1510 cm^{-1}, 1365 cm^{-1}, 1312 cm^{-1}, 1183 cm^{-1}, 769 cm^{-1} and 610 cm^{-1}, which are in good conformity with the reported values [59,60].

When the concentration of R6G was increased, the peak intensity increases. We thus conclude that self-assembled fractal structure of Ag NPs exhibits excellent SERS enhancement as reported earlier [61,62]. This result signifies that self-assembled fractal structure of Ag nanoparticles can be used as SERS active substrate.

4. Conclusions

In summary, resorcinol capped Ag nanoparticles forms hydrogen-bonded nano clusters on silicon wafers by drop casting and evaporating overnight under vacuum. These structures were observed by varying pH from 3 to 11 with optimum pH at 8. Two-dimensional self-assembled fractal structure of Ag NPs appeared on a silicon wafer, occurred due to surface diffusion of atoms dissociated from Ag nanoparticles. The growth formation, morphologies and the fractal structure of Ag NPs strongly depend upon the concentration of $AgNO_3$ and reaction time. R6G has been used as probe molecules for SERS experiments which proved that self-assembled fractal structures of Ag NPs acts as an active substrate and it has high SERS response. The luminescence due to extremely small Ag nanoparticles was also enhanced following a similar pattern of dependence on fractal dimension. The resulting fractal dimension is a complex process of drying of a colloidal solution of Ag NPs formed and capped by resorcinol on a silicon substrate. These Ag nanoparticles form clusters in the solution due to hydrogen bonding, which can be tweaked by the pH of the solution. The tweaking of the pH of the solution after the completion of reduction and capping can affect hydrogen bonding. Additionally, a number of pinning centers and pattern of diffusion on silicon substrate also gets modified by varying the pHs. So, while drying, various different self-similar fractals like structure form on the silicon surface. The surface-enhanced Raman spectrum of model R6G dye and luminescence of ultra-small Ag nanoparticles change in tandem with the varying fractal dimension of the silver structures. This study, therefore, can lead to the development of various sensors based on this optical enhancement relevant to various diverse fields.

Declaration of interest statement

The authors declare that they have no known competing financial interests or personal relationships that could have appeared to influence the work reported in this paper.

Authors agreement

This manuscript demonstrates a strategy to synthesize resorcinol based reduction and capping of ultra-small silver nanoparticles by soft chemical route and a study of their properties. To the best of our knowledge, the results obtained are new and exciting. Specially, the self-assembled luminescent silver nanoparticles are not reported. We believe that "**Optical Materials**" is the most suitable forum for the dissemination of the results contained in this manuscript.

The work described here has not been published before; it is not under consideration for publication anywhere else; and publication has been approved by all co-authors.

Conflicts of interest

The authors declare that they have no conflict of interest.

Funding information

The authors are grateful to GGSIPU, New Delhi for the financial support under the FRGS grant (GGSIPU/DRC/Ph.D./Adm./2017/499) and to DST for FIST grant (SR/FST/PSI-167/2011(C).

Acknowledgment

J.R. Ansari gratefully acknowledges the support from GGSIPU, New Delhi in the form of Short-Term Research Fellowship. The authors are grateful to the Centre for Research in Nanoscience and Nanotechnology, University of Calcutta, India for carrying out TEM characterizations.

Appendix A. Supplementary data

Supplementary data to this article can be found online at https://doi.org/10.1016/j.optmat.2019.05.023.

References

[1] S. Wang, L.-P. Xu, Y. Wen, H. Du, S. Wang, X. Zhang, Space-confined fabrication of silver nanodendrites and their enhanced SERS activity, Nanoscale 5 (2013) 4284, https://doi.org/10.1039/c3nr00313b.
[2] D. T, K.V. Rao, K. Bikshalu, V. Malapati, K.K. Sadasivuni, Non-enzymatic sensing of glucose using screen-printed electrode modified with novel synthesized CeO_2@CuO core shell nanostructure, Biosens. Bioelectron. 111 (2018) 166–173, https://doi.org/10.1016/j.bios.2018.03.063.
[3] J. Dong, S. Qu, H. Zheng, Z. Zhang, J. Li, Y. Huo, G. Li, Simultaneous SEF and SERRS from silver fractal-like nanostructure, Sensor. Actuator. B Chem. 191 (2014) 595–599, https://doi.org/10.1016/j.snb.2013.09.088.
[4] D. Cialla-May, X.-S. Zheng, K. Weber, J. Popp, Recent progress in surface-enhanced Raman spectroscopy for biological and biomedical applications: from cells to clinics, Chem. Soc. Rev. 46 (2017) 3945–3961, https://doi.org/10.1039/C7CS00172J.
[5] X. Xie, H. Pu, D.-W. Sun, Recent advances in nanofabrication techniques for SERS substrates and their applications in food safety analysis, Crit. Rev. Food Sci. Nutr. (2017) 1–14, https://doi.org/10.1080/10408398.2017.1341866.
[6] I. Alessandri, J.R. Lombardi, Enhanced Raman scattering with dielectrics, Chem. Rev. 116 (2016) 14921–14981, https://doi.org/10.1021/acs.chemrev.6b00365.
[7] D. Xu, Y. Zhang, S. Zhang, W. Yang, J. Chen, Solid-state ionics method fabricated centimeter level high surface roughness silver nanoparticles/copper nanowires composites: fractal theory study and SERS application, Opt. Mater. 90 (2019) 194–199, https://doi.org/10.1016/j.optmat.2019.02.047.
[8] M. Kim, W.K. Ham, W. Kim, C.K. Hwangbo, E.H. Choi, G.J. Lee, Optical properties of nucleobase thin films as studied by attenuated total reflection and surface-enhanced Raman spectroscopy, Opt. Mater. 78 (2018) 531–537, https://doi.org/10.1016/j.optmat.2018.03.001.
[9] M.A. El-Aal, T. Seto, M. Kumita, A.A. Abdelaziz, Y. Otani, Synthesis of silver nanoparticles film by spark discharge deposition for surface-enhanced Raman scattering, Opt. Mater. 83 (2018) 263–271, https://doi.org/10.1016/j.optmat.2018.06.029.
[10] H. Jung, C. Park, S. Oh, J.W. Hahn, Nanoscale 2.5-dimensional surface patterning with plasmonic lithography, Sci. Rep. 7 (2017), https://doi.org/10.1038/s41598-017-10047-0.
[11] X.-F. Zhang, Z.-G. Liu, W. Shen, S. Gurunathan, Silver nanoparticles: synthesis, characterization, properties, applications, and therapeutic approaches, Int. J. Mol. Sci. 17 (2016) 1534, https://doi.org/10.3390/ijms17091534.
[12] S. Unser, I. Bruzas, J. He, L. Sagle, Localized surface plasmon resonance biosensing: current challenges and approaches, Sensors 15 (2015) 15684–15716, https://doi.org/10.3390/s150715684.
[13] J. Gong, R. Dai, Z. Wang, Z. Zhang, Thickness dispersion of surface plasmon of Ag nano-thin films: determination by ellipsometry iterated with transmittance method, Sci. Rep. 5 (2015), https://doi.org/10.1038/srep09279.
[14] S. Anjum, G. Jacob, B. Gupta, Investigation of the herbal synthesis of silver nanoparticles using Cinnamon zeylanicum extract, Emergent Mater 2 (2019) 113–122, https://doi.org/10.1007/s42247-019-00023-x.
[15] J.M.J. Santillán, M.B. Fernández van Raap, P. Mendoza Zélis, D. Coral, D. Muraca, D.C. Schinca, L.B. Scaffardi, Ag nanoparticles formed by femtosecond pulse laser ablation in water: self-assembled fractal structures, J. Nanoparticle Res. 17 (2015), https://doi.org/10.1007/s11051-015-2894-8.
[16] I. Gryczynski, E.G. Matveeva, P. Sarkar, S. Bharill, J. Borejdo, W. Mandecki, I. Akopova, Z. Gryczynski, Metal enhanced fluorescence on silicon wafer substrates, Chem. Phys. Lett. 462 (2008) 327–330, https://doi.org/10.1016/j.cplett.2008.08.008.

[17] B. Sardari, M. Özcan, Real-time and tunable substrate for surface enhanced Raman spectroscopy by synthesis of copper oxide nanoparticles via electrolysis, Sci. Rep. 7 (2017), https://doi.org/10.1038/s41598-017-08199-0.

[18] J.-W. Kim, K.-Y. Yang, S.-H. Hong, H. Lee, Formation of Au nano-patterns on various substrates using simplified nano-transfer printing method, Appl. Surf. Sci. 254 (2008) 5607–5611, https://doi.org/10.1016/j.apsusc.2008.03.046.

[19] R.D. Deegan, O. Bakajin, T.F. Dupont, G. Huber, S.R. Nagel, T.A. Witten, Capillary flow as the cause of ring stains from dried liquid drops, Nature 389 (1997) 827.

[20] R.D. Deegan, Pattern formation in drying drops, Phys. Rev. E. 61 (2000) 475–485, https://doi.org/10.1103/PhysRevE.61.475.

[21] M. Grzelczak, J. Vermant, E.M. Furst, L.M. Liz-Marzán, Directed self-assembly of nanoparticles, ACS Nano 4 (2010) 3591–3605, https://doi.org/10.1021/nn100869j.

[22] X. Zhong, F. Duan, Evaporation of sessile droplets affected by graphite nanoparticles and binary base fluids, J. Phys. Chem. B 118 (2014) 13636–13645, https://doi.org/10.1021/jp508051y.

[23] P. Tsai, R.G.H. Lammertink, M. Wessling, D. Lohse, Evaporation-triggered wetting transition for water droplets upon hydrophobic microstructures, Phys. Rev. Lett. 104 (2010), https://doi.org/10.1103/PhysRevLett.104.116102.

[24] X. Zhang, A. Crivoi, F. Duan, Three-dimensional patterns from the thin-film drying of amino acid solutions, Sci. Rep. 5 (2015), https://doi.org/10.1038/srep10926.

[25] M. Hadj-Achour, D. Brutin, Fractal pattern formation in nanosuspension sessile droplets via evaporation-spreading on a glass substrate, Colloids Interface Sci. Commun. 1 (2014) 43–46, https://doi.org/10.1016/j.colcom.2014.06.007.

[26] J. Yang, Z. Jiang, Facile fabrication of dendritic silver structures and their surface enhanced Raman spectroscopic properties, J. Chem. Sci. 127 (2015) 173–176, https://doi.org/10.1007/s12039-014-0763-0.

[27] S. Panigrahi, S. Praharaj, S. Basu, S.K. Ghosh, S. Jana, S. Pande, T. Vo-Dinh, H. Jiang, T. Pal, Self-assembly of silver nanoparticles: synthesis, stabilization, optical properties, and application in surface-enhanced Raman scattering, J. Phys. Chem. B 110 (2006) 13436–13444, https://doi.org/10.1021/jp062119l.

[28] D. Basker, K. Saravanamuttu, Spontaneous formation of fractal aggregates of Au nanoparticles in epoxy-siloxane films and their application as substrates for NIR surface enhanced Raman spectroscopy, Polymers 9 (2017) 507, https://doi.org/10.3390/polym9100507.

[29] G.H. Ma, J. He, K. Rajiv, S.H. Tang, Y. Yang, M. Nogami, Observation of resonant energy transfer in Au:CdS nanocomposite, Appl. Phys. Lett. 84 (2004) 4684–4686, https://doi.org/10.1063/1.1760220.

[30] M. Stockman, Inhomogeneous eigenmode localization, chaos, and correlations in large disordered clusters, Phys. Rev. E. 56 (1997) 6494–6507, https://doi.org/10.1103/PhysRevE.56.6494.

[31] A.V. Butenko, V.M. Shalaev, M.I. Stockman, Fractals: giant impurity nonlinearities in optics of fractal clusters, Z. Phys. At. Mol. Clust. 10 (1988) 81–92, https://doi.org/10.1007/BF01425583.

[32] K. Kneipp, Y. Wang, H. Kneipp, I. Itzkan, R.R. Dasari, M.S. Feld, Population pumping of excited vibrational states by spontaneous surface-enhanced Raman scattering, Phys. Rev. Lett. 76 (1996) 2444–2447, https://doi.org/10.1103/PhysRevLett.76.2444.

[33] K.B. Bhavitha, A.K. Nair, S. Perumbilavil, S. Joseph, M.S. Kala, A. Saha, R.A. Narayanan, N. Hameed, S. Thomas, O.S. Oluwafemi, N. Kalarikkal, Investigating solvent effects on aggregation behaviour, linear and nonlinear optical properties of silver nanoclusters, Opt. Mater. 73 (2017) 695–705, https://doi.org/10.1016/j.optmat.2017.09.024.

[34] A.J. González Fá, A. Juan, M.S. Di Nezio, Synthesis and characterization of silver nanoparticles prepared with honey: the role of carbohydrates, Anal. Lett. 50 (2017) 877–888, https://doi.org/10.1080/00032719.2016.1199558.

[35] H.-J. Schneider, R.K. Juneja, S. Simova, Solvent and structural effects on hydrogen bonds in some amides and barbiturates. An additive scheme for the stability of corresponding host-guest complexes, Chem. Ber. 122 (1989) 1211–1213, https://doi.org/10.1002/cber.19891220631.

[36] W. Kern, Hydrogen Peroxide Solutions for Silicon Wafer Cleaning, RCA Eng, 1983, pp. 99–105.

[37] D.A. Puotinen, W. Kern, Cleaning Solutions Based on Hydrogen Peroxide for Use in Silicon Semiconductor Technology vol. 31, (1970), pp. 187–206.

[38] J.J. Cras, C.A. Rowe-Taitt, D.A. Nivens, F.S. Ligler, Comparison of chemical cleaning methods of glass in preparation for silanization, Biosens, Bioelectron 14 (1999) 683–688, https://doi.org/10.1016/S0956-5663(99)00043-3.

[39] S.I. Bozhevolnyi, V.A. Markel, V. Coello, W. Kim, V.M. Shalaev, Direct observation of localized dipolar excitations on rough nanostructured surfaces, Phys. Rev. B 58 (1998) 11441–11448, https://doi.org/10.1103/PhysRevB.58.11441.

[40] V.A. Markel, V.M. Shalaev, P. Zhang, W. Huynh, L. Tay, T.L. Haslett, M. Moskovits, Near-field optical spectroscopy of individual surface-plasmon modes in colloid clusters, Phys. Rev. B 59 (1999) 10903–10909, https://doi.org/10.1103/PhysRevB.59.10903.

[41] T. Rehm, C. Schmuck, How to achieve self-assembly in polar solvents based on specific interactions? Some general guidelines, Chem. Commun. (2008) 801–813, https://doi.org/10.1039/B710951M.

[42] A. Fatimah, Mohammed, pH responsive hydrogen bonding motif to improve the sensitivity of tumor imaging, https://ir.lib.uwo.ca/etd/1110, (2013).

[43] J. Zheng, Y. Ding, B. Tian, Z.L. Wang, X. Zhuang, Luminescent and Raman active silver nanoparticles with polycrystalline structure, J. Am. Chem. Soc. 130 (2008) 10472–10473, https://doi.org/10.1021/ja803302p.

[44] Y. Ma, K. Promthaveepong, N. Li, Chemical sensing on a single SERS particle, ACS Sens. 2 (2017) 135–139, https://doi.org/10.1021/acssensors.6b00617.

[45] U. Kreibig, M. Vollmer, Optical Properties of Metal Clusters, Springer Berlin Heidelberg, Berlin, Heidelberg, 1995, https://doi.org/10.1007/978-3-662-09109-8.

[46] V.A. Markel, L.S. Muratov, M.I. Stockman, T.F. George, Theory and numerical simulation of optical properties of fractal clusters, Phys. Rev. B 43 (1991) 8183–8195, https://doi.org/10.1103/PhysRevB.43.8183.

[47] A.L. Barabasi, H.E. Stanley, L.M. Sander, Fractal concepts in surface growth, Phys. Today 48 (1995) 68–69, https://doi.org/10.1063/1.2808215.

[48] A. Karperien, FracLac for ImageJ, http://rsb.info.nih.gov/ij/plugins/fraclac/FLHelp/Introduction.htm, (1999).

[49] W.S. Rasband, ImageJ, U. S. National institutes of health, Bethesda, Maryland, USA, 1997https://imagej.nih.gov/ij/.

[50] Q. Zhao, Q. An, J. Qian, X. Wang, Y. Zhou, Insight into fractal self-assembly of poly (diallyldimethylammonium chloride)/sodium carboxymethyl cellulose polyelectrolyte complex nanoparticles, J. Phys. Chem. B 115 (2011) 14901–14911, https://doi.org/10.1021/jp2040423.

[51] J.R. Ansari, N. Singh, S. Mohapatra, R. Ahmad, N.R. Saha, D. Chattopadhyay, M. Mukherjee, A. Datta, Enhanced near infrared luminescence in Ag@Ag2S core-shell nanoparticles, Appl. Surf. Sci. 463 (2019) 573–580, https://doi.org/10.1016/j.apsusc.2018.08.244.

[52] S.L. Smitha, K.M. Nissamudeen, D. Philip, K.G. Gopchandran, Studies on surface plasmon resonance and photoluminescence of silver nanoparticles, Spectrochim. Acta. A. Mol. Biomol. Spectrosc. 71 (2008) 186–190, https://doi.org/10.1016/j.saa.2007.12.002.

[53] K. Jia, P. Wang, L. Yuan, X. Zhou, W. Chen, X. Liu, Facile synthesis of luminescent silver nanoparticles and fluorescence interactions with blue-emitting polyarylene ether nitrile, J. Mater. Chem. C. 3 (2015) 3522–3529, https://doi.org/10.1039/C4TC02850C.

[54] A.S. Kuznetsov, N.T. Cuong, V.K. Tikhomirov, M. Jivanescu, A. Stesmans, L.F. Chibotaru, J.J. Velázquez, V.D. Rodríguez, D. Kirilenko, G. Van Tendeloo, V.V. Moshchalkov, Effect of heat-treatment on luminescence and structure of Ag nanoclusters doped oxyfluoride glasses and implication for fiber drawing, Opt. Mater. 34 (2012) 616–621, https://doi.org/10.1016/j.optmat.2011.09.007.

[55] R. Das, S.S. Nath, D. Chakdar, G. Gope, R. Bhattacharjee, Synthesis of silver nanoparticles and their optical properties, J. Exp. Nanosci. 5 (2010) 357–362, https://doi.org/10.1080/17458080903583915.

[56] L. Maretti, P.S. Billone, Y. Liu, J.C. Scaiano, Facile photochemical synthesis and characterization of highly fluorescent silver nanoparticles, J. Am. Chem. Soc. 131 (2009) 13972–13980, https://doi.org/10.1021/ja900201k.

[57] Y. Chen, T. Yang, H. Pan, Y. Yuan, L. Chen, M. Liu, K. Zhang, S. Zhang, P. Wu, J. Xu, Photoemission mechanism of water-soluble silver nanoclusters: ligand-to-metal–metal charge transfer vs strong coupling between surface plasmon and emitters, J. Am. Chem. Soc. 136 (2014) 1686–1689, https://doi.org/10.1021/ja407911b.

[58] C.D. Geddes, A. Parfenov, D. Roll, I. Gryczynski, J. Malicka, J.R. Lakowicz, Silver fractal-like structures for metal-enhanced fluorescence: enhanced fluorescence intensities and increased probe photostabilities, J. Fluoresc. 13 (2003) 267–276, https://doi.org/10.1023/A:1025046101335.

[59] H.B. Li, P. Liu, Y. Liang, J. Xiao, G.W. Yang, Super-SERS-active and highly effective antimicrobial Ag nanodendrites, Nanoscale 4 (2012) 5082, https://doi.org/10.1039/c2nr30761h.

[60] P. Hildebrandt, M. Stockburger, Surface-enhanced resonance Raman spectroscopy of Rhodamine 6G adsorbed on colloidal silver, J. Phys. Chem. 88 (1984) 5935–5944, https://doi.org/10.1021/j150668a038.

[61] A. González Fá, I. López-Corral, R. Faccio, A. Juan, M.S. Di Nezio, Surface enhancement Raman spectroscopy and density functional theory study of silver nanoparticles synthetized with D -glucose, J. Raman Spectrosc. 49 (2018) 1756–1764, https://doi.org/10.1002/jrs.5466.

[62] J. Bian, Q. Li, C. Huang, Y. Guo, M. Zaw, R.-Q. Zhang, A durable surface-enhanced Raman scattering substrate: ultrathin carbon layer encapsulated Ag nanoparticle arrays on indium-tin-oxide glass, Phys. Chem. Chem. Phys. 17 (2015) 14849–14855, https://doi.org/10.1039/C4CP05803H.